Ternary Complex Crystal Structures of Glycogen Phosphorylase with the Transition State Analogue Nojirimycin Tetrazole and Phosphate in the T and R States[†,‡]

E. P. Mitchell,[§] S. G. Withers,[∥] P. Ermert,[⊥] A. T. Vasella,[⊥] E. F. Garman,[§] N. G. Oikonomakos,[#] and L. N. Johnson*[,§]

Laboratory of Molecular Biophysics and Oxford Centre for Molecular Sciences, University of Oxford, Rex Richards Building, South Parks Road, Oxford OX1 3QU, U.K., Department of Chemistry, University of British Columbia, Vancouver, BC, Canada V6T 1Z1, Laboratory of Organic Chemistry, ETH Zentrum, Universitatstrasse 16, CH 8092 Zurich, Switzerland, and Institute of Biological Research and Biotechnology, National Hellenic Research Foundation, 48 Vas. Constantinou Avenue, Athens 11635, Greece

Received January 11, 1996[⊗]

ABSTRACT: Catalysis by glycogen phosphorylase involves a mechanism in which binding of one substrate tightens the binding of the other substrate to produce a productive ternary enzyme−substrate complex. In this work the molecular basis for this synergism is probed in crystallographic studies on ternary complexes in which the glucosyl component is substituted by the putative transition state analogue nojirimycin tetrazole, a compound which has been established previously as a transition state analogue inhibitor for a number of glycosidases. Kinetic studies with glycogen phosphorylase showed that nojirimycin tetrazole is a competitive inhibitor with respect to glucose 1-phosphate and uncompetitive with respect to phosphate. K_i values for the phosphorylase−AMP−glycogen complex and the phosphorylase−AMP−glycogen−phosphate complexes are 700 μM and 53 μM, respectively, indicating that by itself norjirimycin tetrazole has poor affinity for glycogen phosphorylase but that phosphate substantially improves the binding of nojirimycin tetrazole. X-ray crystallographic binding studies to 2.4 Å resolution with T state phosphorylase *b* crystals showed that nojirimycin tetrazole binds at the catalytic site and promotes the binding of phosphate through direct interactions. Phosphate binding is accompanied by conformational changes that bring a crucial arginine (Arg569) into the catalytic site. The positions of the phosphate oxygens were definitively established in X-ray crystallographic binding experiments at 100 K to 1.7 Å resolution using synchrotron radiation. X-ray crystallographic binding studies at 2.5 Å resolution with R state glycogen phosphorylase crystals showed that the protein atoms and water molecules in contact with the nojirimycin tetrazole and the phosphate are similar to those in the T state. In both T and R states the phosphate ion is within hydrogen-bonding distance of the cofactor pyridoxal 5′-phosphate group and in ionic contact with the N-1 atom of the tetrazole ring. The results are consistent with previous time-resolved structural studies on complexes with heptenitol and phosphate. The structural and kinetic results suggest that nojirimycin tetrazole in combination with phosphate exhibits properties consistent with a transition state analogue and demonstrate how one promotes the binding of the other.

Rabbit muscle glycogen phosphorylase (EC 2.4.1.1) (GP)[1] catalyzes the phosphorolytic cleavage of α-1,4-linked glucose units in glycogen to produce α-D-glucose 1-phosphate (Glc-1-P):

$$\text{glucose}_n + P_i \rightleftharpoons \text{glucose}_{n-1} + \text{Glc-1-P}$$

The reverse reaction, lengthening of the oligosaccharide by addition of the glucosyl moiety of Glc-1-P to the nonreducing end of the α-glucan chain with concomitant production of phosphate, is also catalyzed, and the equilibrium constant for the reaction expressed as the ratio $[P_i]/[\text{Glc-1-P}]$ is 3.6 at pH 6.8. Kinetic experiments indicate that the reaction proceeds through a rapid equilibrium bi-bi kinetic mechanism. There is random addition of substrates, but the binding of one substrate increases the enzyme's affinity for the other substrate. The rate-limiting step in the reaction is the interconversion of the ternary phosphorylase−phosphate−glycosyl complex to the ternary phosphorylase−Glc-1-P−glycosyl complex. These properties have been reviewed (Graves & Wang, 1972). Structural studies on binary complexes of phosphorylase with inhibitors and substrates have provided detailed information on the constellation of key catalytic groups and their relationship to bound substrates (Johnson et al., 1989, 1990). In this work we focus on the ternary enzyme complex through the use of a putative transition state analogue, nojirimycin tetrazole, and phosphate. The studies have led to an understanding of the interactions that provide synergistic binding of the two substrates and the correct localization of the substrate phosphate with respect to the 5-phosphate of the essential

[†] This work has been supported by the MRC and BBSRC (U.K.).

[‡] Coordinates have been deposited with the Protein Data Bank, Brookhaven National Laboratory, Upton NY 11973 (PDB ID codes: 1NOK, 1NOJ, 1NOI).

* Corresponding author. Fax (01865) 510454; Tel (01865) 275365; Email Louise@biop.ox.ac.uk.

[§] University of Oxford.

[∥] University of British Columbia.

[⊥] ETH Zentrum.

[#] National Hellenic Research Foundation.

[⊗] Abstract published in *Advance ACS Abstracts,* May 15, 1996.

[1] Abbreviations: GPb and GPa, rabbit muscle glycogen phosphorylase *b* and phosphorylase *a*, respectively; NJT, nojirimycin tetrazole; BES, *N*,*N*-bis(2-hydroxyethyl)-2-aminoethanesulfonic acid; PLP, pyridoxal 5′-phosphate.

S0006-2960(96)00072-4 CCC: $12.00

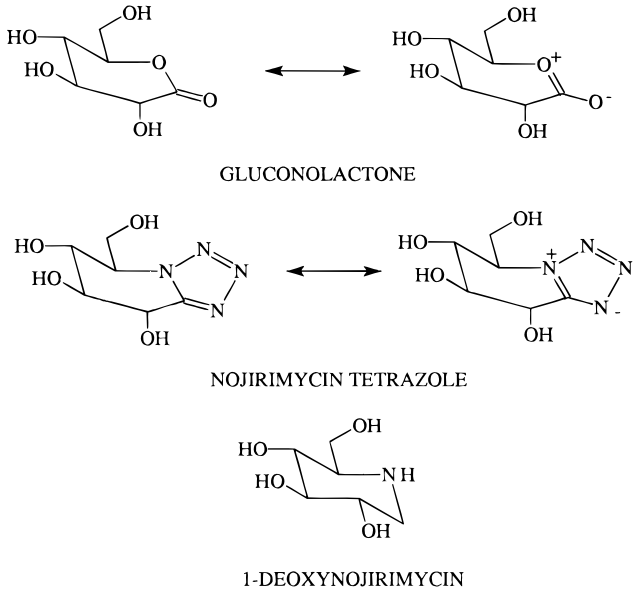

FIGURE 1: Some transition state analogues of glycosidases: D-gluconolactone, nojirimycin tetrazole, and deoxynojirimycin.

cofactor pyridoxal phosphate.

It is anticipated that the glycosyl transfer reaction is likely to have mechanistic similarity to other glycosyl transferases that utilize a double displacement reaction. In these enzymes, a glycosyl−enzyme intermediate is formed and turned over via an oxocarbonium ion-like transition state (Sinnott 1990). Several lines of evidence exist for the involvement of an oxocarbonium ion transition state in the phosphorylase mechanism (Johnson et al., 1989). First, rates of glycogen phosphorylase catalyzed glycosyl transfer with a series of deoxy- and deoxyfluoro-Glc-1-P analogues correlate well with rates of acid-catalyzed hydrolysis of these same substrates (Street et al., 1989). Since the nonenzymatic reaction is known to proceed via an oxocarbonium ion-like transition state, the same should be true for phosphorylase. Second, D-gluconolactone, a compound suggested as an inhibitor of glycosidases (Conchie & Levvy 1957) on the basis of its resemblance to the transition state structure through its flattened chair or sofa-like geometry and its partial charge separation (Figure 1), is also an inhibitor of phosphorylase. However, its affinity for free phosphorylase (apparent dissociation constant K_d = 7.5 mM) is low, suggesting that these geometric and partial charge features by themselves are not sufficient to promote strong binding. The affinity improves 16-fold upon addition of phosphate and a further 18-fold upon addition of glycogen (Gold et al., 1971). Unfortunately, structural studies on D-gluconolactone have been precluded by the hydrolytic instability of this compound.

The activity of phosphorylase is controlled by allosteric mechanisms that involve both noncovalent regulation by effectors, such as the activator AMP and inhibitors glucose and glucose-6-P, and regulation by reversible phosphorylation. X-ray crystallographic structures are available for T state (low affinity, low activity) phosphorylase *b* (GPb) (Acharya et al., 1991) and phosphorylase *a* (GPa) inhibited by glucose (Sprang et al., 1982) and for R state (high activity, high affinity) GPb (Barford & Johnson 1989; Sprang et al., 1991) and GPa (Barford et al., 1991). These studies have shown the changes that take place following activation of the enzyme on conversion from the T to R state either by allosteric effectors or by phosphorylation. The greatest changes in tertiary structure take place at the subunit−subunit contacts, and these shifts lead to shifts of residues at the catalytic site that result in increased access for the large substrate glycogen and the creation of a high-affinity phosphate substrate recognition site. At the catalytic site the displacement of a loop (the 280s loop; residues 282−285) allows the replacement of an acidic residue (Asp283) by a basic residue (Arg569). The conformational changes not only create a high-affinity phosphate site but also promote a favorable electrostatic environment for the 5′-phosphate group of the essential cofactor pyridoxal phosphate (Johnson et al., 1990; Barford et al., 1991). Studies with inhibitors have included a number of ground state analogues such as glucose, Glc-1-methylene phosphate, and glucose-1,2-cyclic phosphate (Withers et al., 1982; Goldsmith et al., 1989; Johnson et al., 1989, 1992; Martin et al., 1990), the dead-end product heptulose 2-phosphate (Johnson et al., 1990), and three glucose derivatives with an sp^2-hybridized anomeric center, heptenitol (McLaughlin et al., 1984; Duke et al., 1994), D-gluconohydroximinolactone *N*-phenylurethane (K_i = 0.4 mM) (Barford et al., 1988), and D-gluconohydroximinolactone (K_i = 0.92 mM) (Papageorgiou et al., 1991). Time-resolved studies on the conversion of the small substrate heptenitol to heptulose 2-phosphate have identified the likely position of the phosphate group in the attacking position in the ternary enzyme−substrate complex (Hadju et al., 1987; Duke et al. 1994). These studies demonstrated that the phosphate group itself provides a major component in the charge stabilization of the oxocarbonium ion transition state. They also showed that the disposition of the substrate phosphate with respect to the cofactor phosphate is critical for promotion of catalysis, in agreement with previous kinetic studies (Parrish et al., 1977; Withers et al., 1981, 1982).

Pyranose compounds in which the ring oxygen is replaced with a nitrogen are potent inhibitors of many glycosidases (Figure 1). For example, deoxynojirimycin exhibits a K_i = 0.032 mM for rabbit intestinal sucrase (Hanozet et al., 1981). Although the precise mechanism by which these compounds inhibit is not fully understood, it is reasonable to assume that the protonatable NH group allows favorable interactions with active site carboxylate groups in glycosidases. At first glance nojirimycin analogues do not appear promising as potent inhibitors for GP. In phosphorylase the ring oxygen of the glucopyranose bound at the catalytic site is in van der Waals contact with two main chain NH groups. These provide a hospitable environment for an oxygen but a less hospitable environment for a NH group. Indeed, deoxynojirimycin itself is a poor inhibitor of phosphorylase [K_i = 55 mM (Ariki & Fukui 1977) compared with a K_i = 1.7 mM for α-D-glucose], and deoxynojirimycin binds poorly in the crystal (L. N. Johnson, unpublished results).

Nojirimycin tetrazole (NJT) has been reported to be a stable, tight-binding inhibitor of several glycosidases (Ermert & Vasella 1991) (Figure 1). In a detailed kinetic analysis of NJT and its 2-epimer as inhibitors of glycosidases and mannosidases (Ermert et al., 1993), a linear relationship between log K_i for each inhibitor/enzyme pair and log k_{cat}/K_m for the equivalent substrate/enzyme pair was established, exactly as required if these inhibitors truly function as transition state analogues. This paper describes the kinetic analysis of the inhibition of phosphorylase by NJT and X-ray binding studies of the binary GPb−NJT complex in the T state and ternary complexes GPb−NJT−phosphate in both T and R states. The kinetic results indicate that phosphate

tightens the binding of NJT, and the X-ray results indicate that NJT tightens the binding of phosphate. An important interaction that underlies the synergistic binding is an interaction between the N1 of NJT and a phosphate oxygen. Correct localization of the phosphate brings it within hydrogen-bonding distance of the cofactor phosphate.

EXPERIMENTAL PROCEDURES

Rabbit muscle GPb was prepared by the method of Fischer and Krebs (1962) using DTT instead of cysteine and recrystallized at least three times before use. Protein concentration was determined from absorbance measurements at 280 nm by using the absorbance index $E_{1cm}^{1\%}$ of 13.2. Rabbit liver glycogen (type III) was purified on a Dowex 1-Cl column and assayed by the method of Dishe (Ashwell, 1957).

Kinetic Studies. Initial reaction rates in the direction of saccharide synthesis were determined at 30 °C by the Fiske−Subbarow phosphate analysis as described (Engers et al., 1970). Reaction mixture volumes were 0.25 mL and contained 1 mM AMP and 0.5% glycogen in pH 6.8 buffer containing 20 mM sodium glycerophosphate, 1.5 mM EDTA, and 5 mM DTT. Initial reaction rates in the direction of glycogen breakdown were determined in the same buffer system using the coupled assay described previously (Engers et al., 1970) in which the product Glc-1-P is converted to glucose 6-phosphate by phosphoglucomutase and then to 6-phosphogluconic acid with conversion of NADP to NADPH, and the reaction is monitored by changes in absorbance at 340 nm. Values for inhibition constants (K_i) were determined by measuring initial reaction rates at a constant concentration of AMP (1 mM) and either glycogen (0.5%) or phosphate (20 mM) with different amounts of the varied substrate and inhibitor as shown in Figure 2. Data were analyzed by the use of the nonlinear regression program GraFit (Leatherbarrow, 1992).

T State Crystallographic Studies. (i) Room Temperature Studies. Data Collection. T state GPb was crystallized from solutions containing 20−40 mg/mL GPb, 1 mM IMP, 1 mM spermine, 10 mM BES, 0.1 mM EDTA, and 0.02% sodium azide (pH 6.7). Crystals are tetragonal, space group $P4_32_12$ with unit cell $a = b = 128.5$ Å and $c = 116.3$ Å. Prior to data collection, native GPb crystals, approximately 1.5 mm × 0.5 mm × 0.5 mm in size, were soaked in a buffered solution (10 mM BES, 0.5 mM EDTA, 0.02% sodium azide, pH 6.7) containing the appropriate ligands (NJT, sodium dihydrogen phosphate) at selected concentrations for 72 h. Data to 2.4 Å resolution were collected on a Siemens X100A multiwire detector with a Rigaku RU-200H rotating anode source using standard protocols (Watson et al., 1995). Each experiment was performed with a single crystal of T state phosphorylase. The data were processed with either the XENGEN (Howard et al., 1987) or XDS (Kabsch, 1993).

Refinement. Structures were refined with X-PLOR (Brunger, 1992). The partial charges used for the glucopyranose ring were those given in the program. Partial charges on the phosphate and tetrazole were estimated from AM1 calculations with MOPAC. The total charge on the phosphate ion was −2.0 with a charge +2.51 on the phosphorus atom, −0.84 on the protonated oxygen (OP-1), +0.15 on the proton, and −1.28 on the three other oxygens. The charges for the tetrazole ring were C-1, +0.24; N-1, −0.08; N-2, −0.13; N-3, −0.04; and N-4, −0.20, where N-1 is the nitrogen common to the sugar and tetrazole rings. For the complex containing NJT alone an established refinement procedure for T state phosphorylase (Watson et al., 1995) was used. The starting model for refinement was the refined structure of the GPb−glucose complex comprising residues 12−841 and including water molecules (Martin et al., 1990), which gave a crystallographic *R* value of 23.7%. A model of NJT, generated using the program SYBYL (Tripos Associates) but almost identical to the single crystal structure (Ermert et al., 1993), was fitted to the density at the active site. The refinement protocol comprised least squares conjugate gradient refinement (200 cycles, tolerance 0.05 Å) followed by individual atomic *B* factor refinement (60 cycles with bond and angle restraints) and gave a final refined model with an *R* value of 19.3%. For the GPb−NJT−phosphate complex, where there were significant conformational changes, a different protocol making use of simulated annealing was used. The initial model was as described above but with the torsion angles of Arg569 adjusted to bring it into the active site. The 280s loop of residues was also adjusted, using the difference map and the refined coordinates of the T state GPb−heptulose 2-phosphate (Johnson et al. 1990) as a guide. Initially the *R* value was 23.8%. Least squares conjugate gradient refinement (100 cycles, tolerance 0.05 Å) was used to prepare the model for simulated annealing. During simulated annealing the structure was heated to 3000 K and gradually cooled to 300 K with a time step of 5 fs and total time of 0.5 ps. Following this further least squares refinement (120 cycles) and individual atomic *B* factor refinement (60 cycles with bond and angle restraints) gave a final *R* value of 15.6%.

(ii) 100 K Studies. Data Collection. T state crystals of phosphorylase were grown as described above. Prior to data collection, crystals (with a maximum size of 0.3 mm on the longest dimension) were soaked for 30 min in a solution containing 100 mM NJT and 50 mM sodium dihydrogen phosphate, 10 mM BES, 0.1 mM EDTA, and 0.02% sodium azide at pH 6.7. Crystals were then transferred to 10 mM BES, pH 6.7, solution containing 50% v/v glycerol as a cryoprotectant for a further 5 min. These soak conditions prior to freezing GPb crystals had been systematically optimized to minimize mosaic spread and to obtain the best resolution diffraction (Mitchell & Garman, 1994). After the second soak, crystals were mounted using the thin loop method of Teng (1990) and flash frozen within 2 s with an Oxford Cryostream cooling device (Cosier & Glazer, 1986) operating with nitrogen gas at 100 K.

Data were collected from a single crystal of GPb prepared as above using a 30 cm diameter MAR Research image plate system which was mounted on the wiggler beamline PX9.6 at the SRS Daresbury. The MAR slits were all set at 0.2 mm, and the X-ray wavelength was 0.895 Å. The crystal to detector distance was set at 250 mm to give a maximum resolution of 1.7 Å at the edge of the detector. Data frames of 0.65° oscillation angle and 100 s exposure time were collected over a total angular range of 88.05°. Data processing was performed with DENZO and SCALEPACK (Otwinowski, 1993). Unit cell dimensions at 100 K were $a = b = 126.7$ Å and $c = 115.6$ Å, giving a 3.5% reduction in unit cell volume from the room temperature crystals.

Refinement. The change in unit cell dimensions on freezing resulted in noisy difference maps that were uninterpretable. X-PLOR refinement, using Engh and Huber parameters (Engh & Huber, 1991) and the electrostatic terms

switched off, began with a starting model of the room temperature structure of the T state GPb−glucose complex comprising residues 12−841 and 633 water molecules (Martin et al., 1990). Least squares conjugate gradient refinement (225 cycles, tolerance 0.05 Å) and restrained individual *B* factor refinement (40 cycles), followed by simulated annealing, heating the structure to 3000 K, and cooling to 300 K with a time step of 5 fs and total time 0.5 ps, and further positional refinement resulted in a drop in the *R* value from an initial 42.1% to 24.0%. At this stage new Fourier difference maps were calculated with SIGMAA (Read, 1986) weighted ($F_o - F_c$) and ($2F_o - F_c$) coefficients. Models of NJT and phosphate were added as indicated by the difference electron density without reference to the refined room temperature structure. The maps contained little density to suggest that the side chain of Arg569 had moved into the active site to coordinate the phosphate ion. The 280s loop of residues was not well supported in the map, but little density was present to suggest a new location. Consequently, the torsion angles of the 280s loop and Arg569 were not adjusted. Further water molecules were identified with PEAKMAX and WATPEAK (CCP4) and the peaks manually screened for sensible positioning, hydrogen bonds, and difference density shape. A total of 144 new water molecules were added to the model, giving an overall total of 777. Several side chains of the enzyme model were adjusted. The refinement continued with a round of positional (70 cycles), individual *B* factor refinement (40 cycles, unrestrained), and a second simulated annealing procedure. This gave an *R* value of 21.0%.

R State Crystallographic Studies. Data Collection. R state GPb crystals (Barford et al., 1989) were obtained from solutions containing 10−12 mg/mL GPb, 1.2−1.4 M ammonium sulfate, 6 mM IMP, 10 mM β-glycerophosphate, 0.5 mM EDTA, 3 mM DTT, and 0.02% sodium azide (pH 7.5). The crystals were then soaked in 1.2 M sodium tartrate, 10 mM β-glycerophosphate, 0.5 mM EDTA, 3 mM DTT, and 0.02% sodium azide (pH 7.0) for 30 min in order to displace the sulfate ion which is bound at the catalytic site when crystals are obtained from ammonium sulfate (Hu, 1992). This was followed by a soak of 3 h in the same solution but with the addition of 25 mM NJT and 25 mM sodium dihydrogen phosphate (pH 7.0). Data were collected at room temperature on an 18 cm MAR Research image plate system mounted on the wiggler beam line PX9.5 at the SRS Daresbury with wavelength 0.90 Å and 0.4 mm diameter collimator. The detector was placed 210 mm away from the crystal to give a maximum resolution of 2.5 Å at the edge of the plate. Data frames of 1.0° oscillation were collected with exposure times of 120 s over a total angular range of 100°. The experiment used a single crystal of R state GPb. Data were processed with DENZO and SCALEPACK (Otwinowski, 1993). The R state GPb−NJT−phosphate crystals are monoclinic, space group $P2_1$ with unit cell dimensions $a = 118.8$ Å, $b = 189.8$ Å, $c = 87.0$ Å, and $\beta = 109.4°$. The unit cell dimensions differed slightly from the native GPb R state values: $a = 119.0$ Å, $b = 190.0$ Å, $c = 88.2$ Å, and $\beta = 109.35°$.

Refinement. The initial model was based upon the refined R state GPb structure, which contained no water molecules and consisted of four monomers each with residues 10−837 (Barford & Johnson, 1989). The coordinates for the sulfates of crystallization from the catalytic and allosteric sites were removed from the coordinate file. The initial *R* value was 34.5% (R_{free} 33.6%). X-PLOR refinement of the complex included 50 cycles of the tetramer as four rigid bodies followed by rigid body refinement of the domains of each subunit. Subsequent refinement constrained the subunits with noncrystallographic symmetry restraints (NCS) of 200 kcal mol^{-1} (300 cycles) on residues which differed by a positional rms deviation of less than 1.0 Å between the four subunits of the tetramer. NCS restraints were loosened to 100 kcal mol^{-1} (140 cycles) to give an *R* value, after individual *B* factor refinement (60 cycles), of 22.9% (R_{free} 29.8%). These coordinates were used to generate new unaveraged difference Fourier electron density maps using SIGMAA ($F_o - F_c$) coefficients, where F_c and the phases were calculated from the refined models above. The significantly improved density was used to place NJT and phosphates at the catalytic sites and phosphates at the Ser14-P and allosteric sites of the tetramer. Further least squares, using NCS restraints of 200 kcal mol^{-1} (150 cycles) and 100 kcal mol^{-1} (40 cycles), and individual *B* factor refinement (80 cycles) reduced the *R* value to 22.1% (R_{free} 28.6%). At this stage water molecules were added to the model, treating each subunit of the tetramer as identical. An averaged Fourier difference map was automatically searched using PEAKMAX for peaks greater than 2.5 times the rms density of the map, and water molecules were assigned to these peaks using the program WATPEAK. The water molecules were independently assigned in the structure without reference to waters in the T state complex. In total of 252 waters were added to each subunit. Further least squares refinement with NCS restraints of 200 kcal mol^{-1} (200 cycles) and 100 kcal mol^{-1} (110 cycles) followed by individual *B* factor refinement (70 cycles) with all ligands and waters in place proceeded. The last stages of refinement with no NCS restraints (90 cycles) and individual *B* factor refinement (50 cycles) gave a final *R* value of 17.1% (R_{free} 27.3%). Such a discrepancy between the crystallographic *R* value and free *R* value at 2.5 Å resolution is not untypical (Brunger, 1992).

Analysis of Structures. Structures were analyzed with the graphics programs FRODO (Jones, 1985) and O (Jones et al., 1991). Hydrogen bonds were noted between polar groups if the relevant atoms were separated by less than 3.3 Å and the angles formed between the atoms and the preceding atom were greater than 90°. Van der Waals interactions were noted where the separation between non-hydrogen atoms was less than 4 Å. Superposition of structures was performed with the LSQ option in O.

RESULTS

Kinetics. NJT exhibited competitive inhibition with respect to the substrate Glc-1-P when the reaction was assayed in the direction of glycogen synthesis, yielding a K_i value of 700 μM for binding to the GPb−AMP−glycogen complex as shown in Figure 2a. When assayed in the direction of glycogen breakdown with variable concentrations of NJT and phosphate, the results shown in Figure 2b were observed, which are most simply interpreted as indicating uncompetitive inhibition. This model gave the best fit to the data, yielding a K_i value of 53 μM for binding to the GPb−AMP−glycogen−P_i complex. The data could also be interpreted as indicating mixed inhibition, but this would not change the major conclusion of this part of the study that the presence of phosphate dramatically improves the affinity for NJT. Noncompetitive inhibition was observed when GP

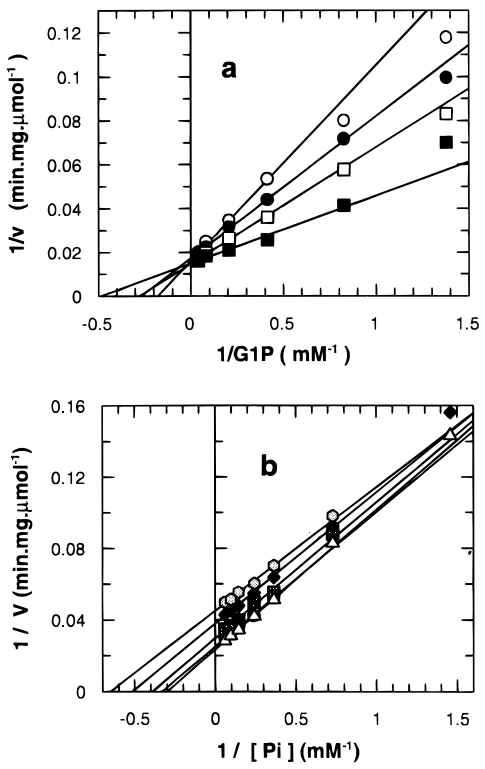

FIGURE 2: Lineweaver−Burk plots for phosphorylase catalysis. (a) Competitive inhibition by NJT of GP assayed in the direction of glycogen synthesis. Concentrations of NJT used were 0, 0.37, 0.75, 1.3, 1.9, and 3.7 mM, and concentrations of Glc-1-P used were 0.7, 1.2, 2.4, 4.8, 12.1, and 24.2 mM. Curves for the last two concentrations of NJT are not shown. (b) Uncompetitive inhibition by NJT of GP assayed in the direction of glycogen breakdown. Concentrations of NJT used were 0, 5, 15, 30, and 50 μM, and concentrations of phosphate used were 0.7, 1.4, 2.7, 4.1, 6.9, 10.3, and 16.5 mM. For further details see text.

was assayed in the direction of glycogen breakdown with varying glycogen concentrations and a K_i of 59 μM obtained. Thus again the binding of NJT to a complex containing phosphate is reasonably tight.

T State Crystallographic Studies. (1) Room Temperature. Binding sites on GP have been previously defined (Johnson et al., 1989; Johnson, 1992). The catalytic site is situated in the center of the phosphorylase subunit and is buried some 12 Å from the surface. Access to the catalytic site is via a channel, and in the T state the channel is partly blocked by the 280s loop. Glycogen phosphorylase contains a nucleoside inhibitor site at the entrance to the catalytic site channel which is located some 12 Å from the catalytic site. The site also binds a number of aromatic compounds, such as caffeine. The inhibitors intercalate between the aromatic rings of Phe285 and Tyr613 and partially block access to the catalytic site. Binding of ligands at the inhibitor site promotes localization of the 280s loop in its inactive T state conformation and prevents conformational changes that lead to the active high-affinity R state conformation. The allosteric effector site is over 30 Å from the catalytic site and is situated at the subunit−subunit interface of the dimer molecule. This site binds the allosteric effectors such as AMP and glucose-6-P, and a major part of the binding specificity is directed by the contacts from the phosphate groups to two adjacent arginine residues, Arg309 and Arg310.

Crystallographic data collection statistics and refinement for two of the complexes (100 mM NJT and 1 mM NJT plus 50 mM phosphate) are shown in Table 1. A number of experiments were carried out with different concentrations of ligands. A summary of the sites occupied in the binding experiments is given in Table 2. The X-ray data collection statistics and refinement results for complexes 2−5 and 7−8 are not shown. These are very similar to those for complexes 1 and 6 (Table 2) which are described in detail (Table 1).

In experiments with 100 mM NJT and 100 mM NJT plus 1 mM phosphate, electron density difference maps showed that there was strong binding of NJT at the catalytic site, weak binding of NJT at the nucleoside inhibitor site, and no movement of the 280s loop (Table 2). No phosphate was bound at the catalytic site. With 100 mM NJT and a high concentration of phosphate (50 mM), both NJT and phosphate were bound at the catalytic site; there was weak binding of NJT at the inhibitor site and some indication of shifts in the 280s loop. Experiments with lower concentrations of NJT showed that, at 1 mM NJT, 50 mM phosphate NJT bound at the catalytic site but not at the inhibitor site and there was movement of the 280s loop and strong binding of phosphate at the catalytic site. In all experiments in which phosphate was present, phosphate bound at the allosteric site. Thus it was possible to establish conditions in which NJT bound at the catalytic site but not at the inhibitor site.

Phosphate binding at the catalytic site showed a dependence on phosphate concentration and binding of NJT at the catalytic site (Table 2). At 1 mM phosphate there was no binding of phosphate at the catalytic site in the presence of either 100 mM or 1 mM NJT. As the concentration of phosphate was increased in the presence of 1 mM NJT, binding was observed at concentrations of phosphate 10 mM or higher (Table 2). In contrast, in the absence of NJT there is no binding of phosphate at 50 mM concentration, a result consistent with previous experiments that had shown that even at 500 mM phosphate there is no binding of phosphate at the catalytic site in the absence of substrate (Hadju et al., 1987). Likewise, no binding of phosphate is observed at the catalytic site in the presence of glucose. Thus there is a good correlation between binding of NJT at the catalytic site and binding of phosphate at the catalytic site. There is also a correlation between negligible binding of NJT at the inhibitor site (achieved with low concentrations of NJT) and shifts in the 280s loop. We describe in detail the binary complex with 100 mM NJT and the ternary complex obtained with the low concentration of NJT (1 mM) and 50 mM phosphate.

Interactions between NJT and GP. NJT binds in an identical position at the catalytic site in the binary GPb−NJT and the ternary GPb−NJT−phosphate complexes. The rms deviation between the coordinates for NJT in the two complexes is 0.22 Å, which is similar to the precision in the coordinates (Acharya et al., 1991). The position of the sugar moiety is almost identical to the position of glucose bound at the catalytic site (Martin et al., 1991). The hydrogen bonds and van der Waals contacts are summarized in Tables 3 and 4 and are illustrated in Figure 3a. There are specific hydrogen bonds from each of the peripheral hydroxyl groups O-2, O-3, O-4, and O-6 to groups on the enzyme. The hydrogen bond from the main chain NH of Leu136 to the N-2 atom tetrazole ring is bent. The nitrogen N-1 is 3.9 Å from the NH of Leu136, and the anomeric carbon C1 is close (3.3 Å) to the main chain carbonyl oxygen of His377. The tetrazole ring is sandwiched between residues Leu136, Asn284, Asp339, His377, and Thr378 and fits neatly into

Table 1: Statistics of Data Collection, Processing, and Refinement

	room temp T state GPb		100 K T state GPb	room temp R state GPb
ligand	100 mM NJT	1 mM NJT, 50 mM P_i	100 mM NJT, 50 mM P_i	25 mM NJT, 25 mM P_i
no. of measured reflections	82739	72437	304397	263189
no. of unique reflections	37024	27392	88768	107826
% completeness of data (resolution)	95 (∞−2.4 Å)	70 (∞−2.4Å)	86 (∞−1.7 Å)	88 (∞−2.5 Å)
% completeness of highest resolution shell	81 (2.56−2.40 Å)	51 (2.56−2.4 Å)	67 (1.76−1.70 Å)	74 (2.56−2.50 Å)
$R_m(I)$[a] (%)	6.8	6.1	4.9	7.0
no. of reflections $I/\sigma > 3$	21273	19203		
ratio I/σ			19	14
R_{iso}[b] (%)	11.7	13.6	NA	36.1
no. of protein atoms in refinement	6780	6780	6755	26768
no. of ligand atoms	14	24	19	96
no. of waters in final cycle	569	568	777	1008
no. of reflections used in refinement ($I > 0$)	36005	26563	84349	104617
resolution range for refinement	8.0−2.4 Å	8.0−2.4 Å	5.0−1.7 Å	8.0−2.5 Å
initial R value[c] (%) (R_{free})	23.7	23.8	42.1	34.5 (33.6)
final R value[c] (%) (R_{free})	19.3	15.6	21.0	17.1 (27.3)
rms deviation in bond lengths (Å)	0.017	0.016	0.008	0.018
rms deviation in bond angles (deg)	3.2	3.1	1.4	3.4
rms differences in B factors for bonded atoms (Å^2)	3.0	3.3	4.7	2.8
estimated coordinate error (from Luzzatti or SIGMAA plots) (Å)	0.25−0.3	0.25−0.3	0.13	0.3−0.35

[a] R_m is merging $R = \sum_i\sum_h[|I(h) - I_i(h)|]/\sum_i\sum_h[I(h)]$, where $I_i(h)$ is the ith measurement of reflection h and $I(h)$ is the mean intensity for that reflection. [b] R_{iso} is the mean fractional isomorphous difference of structure factor amplitudes of the ligand−protein complex and the native protein. NA, not applicable; the frozen T state crystals were nonisomorphous with the native enzyme. [c] R value is the crystallographic R value $= \sum||F_o| - |F_c||/\sum|F_o|$, where $|F_o|$ and $|F_c|$ are the observed and calculated structure factor amplitudes, respectively. R_{free} is the corresponding R value for 5% of the reflections that were not included in the refinement.

Table 2: Summary of Sites Occupied in Four Different Concentrations of NJT and Phosphate

	ligand concn		binding sites occupied[a]				
			catalytic inhibitor		allosteric inhibitor		
expt	NJT (mM)	phosphate (mM)	NJT	phosphate	phosphate	NJT	shift in 280s loop?
1	100	0	+	−	−	+	no
2	100	1	+	−	+	+	no
3	100	50	+	+	+	(+)	partial
4	1	1	+	−	+	−	no
5	1	10	+	(+)	+	−	partial
6	1	50	+	+	+	−	yes
7	0.1	50	+	+	+	−	yes
8	0	50	−	−	+	−	no

[a] A + denotes site occupied; parentheses indicate partial occupancy as estimated from the appearance of electron density peaks. A − denotes site not occupied.

the "β pocket", a space adjacent to the C1 position that has been the target for a number of glucose analogue inhibitors (Martin et al., 1991; Watson et al., 1994, 1995; Bichard et al., 1995). In the most potent glucose analogue inhibitor complexes, the carbonyl oxygen of His377 makes a strong hydrogen bond to the nitrogen in the β-substituted acetamido sugar complexes and in the hydantoin complex.

Conformational Changes. In the binary GPb−NJT complex the conformational changes in the enzyme are small and similar to those observed when glucose binds. There is a small shift in the position of His377 away from the sugar in order to optimize contacts to O-6. The main chain and side chain of Leu136 shift about 0.5 Å in order to accommodate the tetrazole ring.

Inclusion of phosphate in the ternary GPb−NJT−phosphate complex results in movement of the 280s loop and Arg569. The rms deviation of the catalytic site residues (residues 88, 132−137, 281−286, 376−384, 568−574, 613, and 671−676 and PLP) in the ternary complex from their positions in the native enzyme is 1.36 Å compared with 0.63 Å observed for the binary complex. The greatest shifts are made by Arg569 where the side chain rotates by 154° about the Cα−Cβ bond and the NH1 and NH2 atoms shift by 7 Å into the catalytic site (Figure 3b). Both Arg569 and the 280s loop are less well defined in the ($2F_o - F_c$) Fourier map density of the ternary complex compared to the rest of the residues at the catalytic site, and the disorder is apparent in the increased temperature factors. Residues 281−286 have a mean B factor of 39 Å^2 compared to that of 24 Å^2 for all the residues of the catalytic site. In moving from its native buried location, Arg569 breaks four hydrogen bonds and in its new position makes up to three new hydrogen bonds to catalytic site residues, as well as making ionic contacts from the guanidinium group to substrate phosphate (described later). There are small shifts in main chain atoms between residues 282 and 285 and substantial rearrangements in the side chains of Asp283 and Asn284. Part of the space vacated by these residues is occupied by Arg569 (Figure 3b). Asp283 in its new position makes similar contacts to those of Arg569 in the native structure, namely, hydrogen bonds to the main chain oxygens of Lys608 and the side chain of Asn133, and these contacts require the residue to be protonated. Asn284 moves out of the catalytic site by some 4 Å, with displacement of a water molecule. The hydrogen bond between O-2 of the glucosyl ring and ND2 Asn284, found in the GPb−NJT complex, is no longer formed. In

Table 3: Polar Contacts (Å) between NJT and Phosphate and Residues at the Catalytic Site of GPb

		room temperature T state GPb (2.4 Å)		100K T state GPb (1.7 Å)	R state GPb (2.5 Å) subunits 1, 2, 3, 4
ligand atom	protein atom	NJT	NJT + P_i	NJT + P_i	NJT + P_i
		Nojirimycin Tetrazole			
O-2	ND2 Asn284	3.2	−	−	NA
	OH Tyr573	3.2	3.0	2.9	2.9, 3.0, 2.9, 2.7
	OE1 Glu672	3.1	3.2	3.1	3.1, (3.5), 3.1, 3.2
	OH7 Wat890	2.9	3.0	2.7	2.9, 2.6, 2.9, 2.7
	OP-2 Phos	NA	3.0	2.7	2.8, 3.1, 2.8, 2.9
O-3	OE1 Glu672	2.8	2.8	2.9	2.7, 2.7, 2.8, 2.6
	N Ala673	−	3.3	3.3	(3.5), (3.5), (3.6), 3.1
	N Ser674	3.1	3.1	2.9	3.3, 3.3, 3.3, 3.1
	N Gly675	3.1	3.2	3.1	3.0, 3.2, 2.9, 3.3
O-4	N Gly675	2.8	2.8	2.7	3.0, 2.9, 2.9, 2.9
	OH1 Wat897	2.7	2.7	2.7	2.6, 2.6, 2.7, 2.7
O-6	ND1 His377	2.7	2.6	2.6	2.7, 2.9, 2.8, 2.7
	OD1 Asn484	2.9	2.8	3.1	−
	ND2 Asn484	−	−	−	3.0, 2.7, 3.0, (3.4)
N-1[a]	OP-1 Phos	NA	3.1	−	3.0, 3.2, 3.1, 3.1
N-2	N Leu136	3.3	(3.4)	3.1	3.1, (3.5), (3.4), (3.5)
N-3	ND2 Asn284	−	3.1	−	NA
	OH2 Wat73[b]	2.8, 3.1, 2.7, 2.9			
N-4	OD1 Asn284	−	−	2.6	NA
	OG1 Thr378	3.3, 2.6, (3.5), 2.9			
		Phosphate			
OP-1[a]	N-1 NJT	NA	3.2	2.8	3.0, 3.2, 3.1, 3.3
	N Gly135	NA	−	−	3.0, 3.2, 3.1, 3.2
	OH2 Wat70[b]	NA	NA	2.8	2.5, 2.5, 2.6, 2.5
OP-2	O-2 NJT	NA	3.0	2.7	2.9, 3.1, 2.8, 3.0
	NH1 Arg569	NA	(3.4)	−	3.3, (3.4), 3.2, 3.0
	OH Tyr573	NA	3.3	3.3	3.2, 3.2, 3.3, (3.4)
	NZ Lys574	NA	3.3	3.2	2.8, 3.1, 2.9, 3.0
	ND2 Asn284	NA	−	2.8	NA
OP-3	OP-2 PLP	NA	2.7	3.0	2.5, 2.5, 2.8, 2.6
	OH1 Wat897	NA	2.7	2.7	2.7, 2.7, 2.8, 2.8
OP-4	N Gly135	NA	3.1	2.7	3.0, 2.9, 2.9, 2.8
	NE Arg569	NA	−	−	3.3, (3.4), 3.3, 3.3
	OH0 Wat879	NA	2.8	2.5	2.5, 2.8, 2.8, 2.6
	OH0 Wat887[c]	NA	2.7	−	NA

[a] Contact represents an electrostatic interaction. [b] This water molecule is not observed in the T state. [c] This water molecule is not observed in the R state. Waters are numbered differently in the 100 K 1.7 Å and R state structures but are spatially equivalent. NA, not applicable either because phosphate is not present (as in the binary 100 mM NJT complex) or because the 280s loop, including Asn284, has shifted from the catalytic site. A dash indicates contact greater than 3.3 Å. Some important longer contacts are noted in parentheses.

its new position, Asn284 is directed toward Asp339 and makes a hydrogen bond to Wat891, which in turn contacts a buried histidine, His341. In the native enzyme, another histidine, His571, is hydrogen bonded to Asp283. In the ternary complex His571 makes a small conformational change and rotates by 60° in order to make a hydrogen bond to the new position of the main chain oxygen of Asp283. There is no conformational change in the cofactor PLP between the native enzyme and the complexed structures. The inhibitor site, formed by the aromatic side chains of Phe285 and Tyr613, is intact and is similar to the native conformation.

The changes in the 280s loop and in Arg569 are accomplished with no change in the subunit−subunit contacts. The tower helices and the cap-α2 helix contacts in the N-terminal region of the molecule have the same positions as in the native T state GPb. In the T state crystals the subunit contacts are also symmetry-generated lattice contacts. Thus the changes at the catalytic site in the ternary complex, which are characteristic of the changes on the conversion of an inactive to an active enzyme, are accomplished without the change in quaternary structure that accompanies the T to R transition. The failure of the enzyme to respond with a quaternary structure change is probably due to the lattice contacts which impede such changes. A similar result was observed for the heptulose 2-phosphate complex (Johnson et al., 1990).

Interactions between Phosphate, NJT, and Catalytic Site Residues. In the ternary complex, the phosphate binds between the 5′-phosphate group of the PLP and the tetrazole ring (Figure 3c). The phosphate makes a total of 9 hydrogen bonds (Table 3) and 44 van der Waals interactions, of which 27 are to protein atoms, 7 to the PLP, and 10 to NJT (Table 4). The phosphorus−phosphorus distance between the phosphate and 5′-phosphate of PLP is 4.7 Å. There is a direct hydrogen bond between the two phosphate oxygens. Such an intimate interaction of negatively charged groups requires compensating neighboring residues. This is provided by the basic side chains of Lys568, Lys574, and Arg569 (in its new position). Lys574 shifts slightly toward the cofactor phosphate and lies equidistant between the two phosphates making hydrogen bonds to both phosphates. The contacts to Arg569 are rather long for a strong hydrogen bond, but there is a hydrogen bond from OP-4 through Wat887 to Arg569. The two well-ordered water molecules, Wat879 and Wat897, form a bridge between the phosphate oxygens so that there is a network of extensive interactions (Figure 3c).

There is a direct contact between the inorganic phosphate and the NJT (Table 3). The phosphate interacts with NJT

Table 4: Van der Waals Contacts between NJT and Phosphate and GPb

	room temperature T state 2.4 Å	
	NJT	NJT + Pi
	Nojirimycin Tetrazole	
C-1	His377 (CB, O)	His377 (CB, O), Phos (OP-1, OP-2)
C2	Glu672 (OE1), Wat890 (OH7)	His377 (O), Glu672 (Oe1), Wat890 (Oh7), Phos (Op-1, Op-2)
O-2	Asn284 (CG, OD1)	Arg569 (NH2), Phos (O1)
C-3	Glu672 (OE1), Gly675 (N), Wat897 OH1	Glu672 (OE1), Gly675 (N), Wat897 (OH1), Phos (OP-2, OP-3)
O-3	Glu672 (CG, CD), Ser674 (O, CA), Gly675 (CA), Wat890 (OH7)	Glu672 (C, CG, CD), Ala673 (N, CA, C, CB), Ser674 (CA, C, N), Gly675 (CA), Wat890 (OH7)
C-4	Asn484 (OD1), Gly675 (N), Wat897 (OH1)	Asn484 (OD1), Gly675 (N), Wat897 (OH1)
O-4	Asn484 (OD1), Ser674 (C, CB), Gly675 (CA, C, O)	Asn484 (OD1), Ser674 (CB), Gly675 (CA, C, O)
C-5	Gly135 (C), Wat897 (OH1)	Wat897 (OH1), Phos (OP-1)
C-6	Gly135 (C, O), Leu139 (CD2), His377 (ND1), Asn484 (OD1), Wat897 (OH1)	Gly135 (O), His377 (ND1, CE1), Asn484 (OD1)
O-6	Leu139 (CD2), His377 (CG, CE1), Val455 (CG1), Asn484 (CG, ND2)	His377 (CG, CE1), Val455 (CB, CG1), Asn484 (CG, ND2)
N-1	Leu136 (N), His377 (ND1)	His377 (ND1), Phos (OP-1)
N-2	Gly135 (C), Leu136 (CA, CB, CD1), His377 (CB, CG, ND1)	Gly135 (C), Leu136 (N, CA, CB,CD1), His377 (CB, CG, ND1)
N-3	Leu136 (CD1), His377 (CB, CG, ND1)	Leu136 (CB), His377 (CB, CG), Phos (OP-1)
N-4	His377 (CB, O), Asn484 (OD1, ND2)	Asn284 (ND2), His377 (O, CB), Phos (OP-1)
	Phosphate	
P		Gly135 (N, CA), Arg569 (CZ), Wat879 (OH0), Wat887 (OH0), PLP (OP-2)
OP-1		Gly135 (N, CA, C), Leu136 (N), Arg569 (NH2), Wat897 (OH0), NJT (O2, C5, N1, N2, N3, N4)
OP-2		Arg569 (CD, NE, CZ, NH1, NH2), Tyr573 (OH), Lys574 (CE, NZ), PLP (OP-2), NJT (C1, C2, C3)
OP-3		Gly135 (N, CA), Wat879 (OH0), PLP (C5, P, OP-3, OP-4), NJT (C3)
OP-4		Gly135 (CA, C), Arg569 (CD, NE, NH2), PLP (OP-2)

in two ways. A hydrogen bond is formed between OP-2 of the phosphate and the O-2 hydroxyl of the glucopyranose ring. The second contact is an interaction between OP-1 and N-1 of the tetrazole ring. The separation of OP-1 to N1 is 3.2 Å and from OP-1 to C1 is 3.3 Å.

(ii) 100 K Studies. Freezing GPb crystals allowed high-resolution data to be collected, and the experiments were carried out with the aim of establishing the precise orientation of the phosphate oxygens at the catalytic site. After refinement, the density of the ($2F_o - F_c$) Fourier map suggested partial occupancy of the active site by NJT. In the 1.5 Å structure of the native enzyme at 100 K (results not shown) glycerol, used as a cryoprotectant, was bound to the catalytic site. The partial occupancy of NJT probably results from competition for the catalytic site by glycerol. Uhing et al. (1979) have observed a 13% inhibition of GPb activity by 10% glycerol determined at saturating conditions. Occupancies were not refined against the 1.7 Å data as there was likely to be too great a correlation with temperature factors. Some measure of the relative occupancies can be obtained by comparing temperature factors at room temperature and 100 K for the ligands with those for the PLP 5′-phosphate group, with the expectation that normalizing to a nearby group of the protein might remove some of the errors inherent in comparing temperature factors of structures determined to different resolutions and at different temperatures. The *B* factors for the cofactor 5′-phosphate, inorganic phosphate, and NJT were in the ratio 1:2.2:1.4 for the room temperature 2.4 Å data and were in the ratio 1:2.3:2.3 for the 100 K 1.7 Å resolution data. These ratios suggest that the phosphate is present at roughly the equivalent occupancy in the room temperature and 100 K structures but that the NJT is at a lower occupancy, perhaps as low as 60%, in the 100 K structure. These conclusions are supported by the electron density which shows strong density for the phosphate and less satisfactory density for the NJT (Figure 4).

Despite the low occupancy of NJT, the density was sufficiently well resolved to indicate the positions of the NJT and the phosphate ion orientation. A comparison of the refined structure with that of the equivalent room temperature complex shows the phosphate to be in the same orientation in the higher resolution structure. The positions of Arg569 and the 280s loop were not remodeled from their native positions in the higher resolution structure because, although there was some indication of less than satisfactory density for Asn284 and a shift in His571, there was little indication of new positions. There was no binding of NJT at the inhibitor site. The closest contact from the Asp283 oxygen to the phosphate oxygen is 3.6 Å. With the exception of these contacts, both NJT and phosphate make similar contacts in the models derived from the room temperature and flash-frozen data (Table 3). The lengths of the contacts show some variation but are within the coordinate experimental error of the 2.4 Å structure (0.20−0.30 Å). The results from this structure at 1.7 Å resolution establish the orientation of the phosphate oxygens and confirm the positions deduced from the earlier results and refinement.

R State Crystallographic Studies. Monoclinic crystals of R state GPb contain a tetramer in the asymmetric unit. The tendency of R state GP to associate from the more active dimeric state to the less active tetrameric state results from changes in surface groups of the enzyme on activation (Barford & Johnson, 1992). These changes include movements in part of the glycogen storage site. The R state crystals have been shown to be active with kinetic similar properties to those of the enzyme in solution (Leonidas et al., 1992). R state crystals of both GPb and GPa grown in the presence of ammonium sulfate have a sulfate ion bound at the catalytic site. In the present work the crystals were soaked in tartrate in order to diffuse out the sulfate ion from

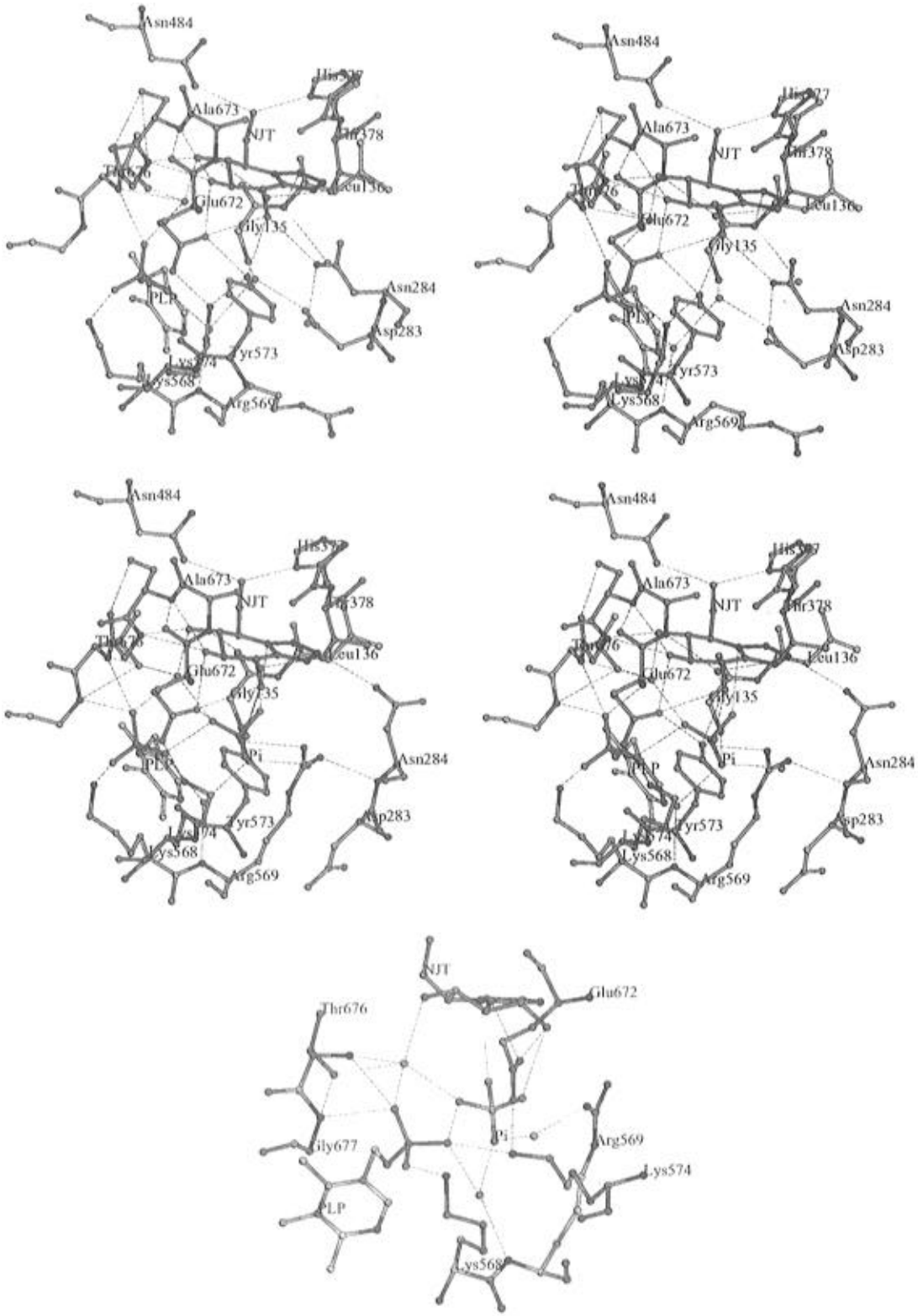

FIGURE 3: Contacts between NJT and phosphate and protein groups at the catalytic site of T state GPb. NJT and protein carbon atoms are shown in green and yellow, respectively. O, N, and P atoms are in red, blue, and magenta, respectively. (a, top) Binary NJT−GPb complex. (b, center) Ternary GPb−NJT−phosphate complex. The movements of Arg569 and the 280s loop on binding phosphate are apparent from comparison of (a) and (b). (c, bottom) Details of the phosphate and PLP 5′-phosphate interactions in the GPb−NJT−phosphate complex. There is one direct phosphate oxygen−phosphate oxygen contact and two further contacts through water molecules. Gly135 and Tyr573 have been omitted for clarity. The contact from Lys574 to O2 is just over 3.3 Å and has not been drawn.

the catalytic site and to allow the phosphate to bind.

The data collection and refinement statistics for the R state GPb−NJT−phosphate complex at 2.5 Å resolution are shown in Table 1. The refined structure of the complex showed that both NJT and phosphate were bound at the catalytic site. Phosphate ions were also bound at the anionic allosteric and Ser14-P sites in positions which were close to, but not identical to, those observed for sulfate ion binding in native R state GPb. The individual subunits of the tetramer of the complex are similar (rms deviation of 820 Cα atoms between subunits 1 and 2 is 0.59 Å, 1 and 3 is 0.55 Å, and 1 and 4 is 0.61 Å). The differences in positions, averaged over the four subunits, of the 5′ phosphorus atoms of PLP and of the phosphorus positions of the phosphate

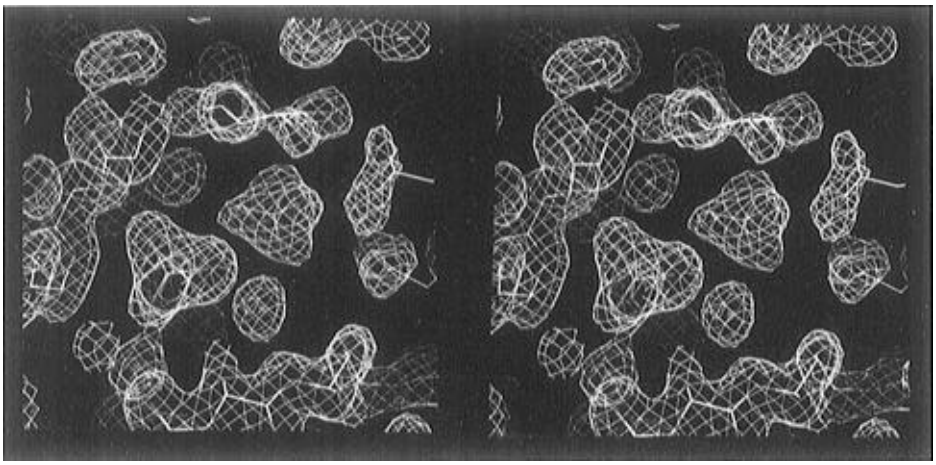

FIGURE 4: Electron density from the final $2F_o - F_c$ map for the 1.7 Å structure of the GPb−NJT−phosphate complex at 100 K showing the density in the vicinity of the cofactor phosphate, the substrate phosphate, and the NJT. Contour levels correspond to 1σ.

ions are 0.14 and 0.20 Å, respectively. The overall tertiary and quaternary structure of the GPb−NJT−phosphate complex is similar to that of native R state GPb and R state GPa structures. [The structure of R state GPa is more precise than that of R state GPb (Barford et al., 1991), and we therefore use the GPa structure for the detailed comparisons.] The rms deviation over all Cα atoms between the native GPa structure (2.8 Å resolution) and the GPb−NJT−phosphate complex structure (2.5 Å resolution) is 0.7 Å. The largest positional deviations between the native and complexed structure are for those residues that are poorly located in density and exhibit high *B* factors: i.e., residues 211−212, 250−263, and 313−320. These regions are also poorly located in the native R state structures (Barford et al., 1991). However, despite the overall similarity between the native and complexed structures there are some differences in the region of the catalytic site. The rms deviation of Cα atoms between native and complexed enzyme for all atoms within 10 Å of the phosphate ion is 1.4 Å. The shifts mostly arise from Arg569, whose movement is correlated with the displacement of a sulfate ion, and from shifts in the 380s loop (residues 378−384).

In R state GPb and GPa, a dianionic site at the catalytic site is already formed, promoted by the tertiary and quaternary changes from the T to the R state. The sulfate ion, bound at the catalytic site in the native crystals, is hydrogen bonded by Arg569, Lys574, and the PLP 5′-phosphate (the P−P separation = 5 Å) (Barford et al., 1989). In the GPb−NJT−phosphate complex, a phosphate ion is bound at the catalytic site (Figure 5a). The phosphate binding site in the complex appears to be a tighter binding site than the native sulfate binding site. The average *B* factor for the phosphate ion is 21 Å^2 (2.5 Å resolution) in the GPb−NJT−phosphate complex compared to 61 Å^2 (2.8 Å resolution) for the sulfate ion in the native structure, although the different resolutions of the two structures mean that a detailed *B* factor comparison is not valid. The distance between the phosphate ion in the complex and the sulfate ion in the native structure (P−S distance) averaged over each of the four subunits in both structures is 2.5 Å. The cofactor 5′-phosphate group shifts slightly away from the phosphate ion in the complex, and the shift averaged over each of the four subunits is 0.7 Å. The movement of the PLP group between native and complexed R state GPb is accompanied by shifts of Thr676 and Gly677 so that the main chain nitrogens of these residues make shorter hydrogen bonds with the 5′-phosphate. These conformational changes are also accompanied by smaller movements around the catalytic site of other side chains and main chain atoms (Figure 5b).

On binding to the phosphate ion, Arg569 shifts toward the phosphate so that it occupies a position close to that of the sulfate ion in the native structure. The average shift is 2.5 Å for the CZ atom. In its new position the guanidinium group of Arg569 makes two contacts to the phosphate ion. In total, the phosphate ion makes seven hydrogen bond contacts to the protein and two contacts to NJT (Table 3). A recent review of phosphate and sulfate binding sites (Copley & Barton, 1994) showed that phosphate ions on average make 3.5 contacts to protein residues in the 38 proteins studied. This suggests the R state phosphate ion, which makes seven contacts to protein groups and a further four contacts to waters and NJT, is tightly coordinated.

The glucosyl recognition pocket at the R state catalytic site is almost identical to that in the T state enzyme, and the contacts made by NJT are very similar (Figure 5a and Table 3). The phosphate ion is bound nearby, and the contacts from the phosphate to O-2 and N-1 of the tetrazole are similar to those observed in the T state complex. The torsion angles of Glu672 are adjusted, and the carboxyl oxygens make two hydrogen bonds to O-2 and O-3 of the tetrazole and one to the OH of Tyr573 (Table 3). There is a significant shift in residues 378−384 between the complex and native R state structures (Figure 5b). In particular, the side chain of Thr378 is directed in toward NJT and contributes a polar interaction with the N-4 atom of NJT (Table 3) (with the exception of subunit 3 where the shift is less marked). The average shift for the OG1 atom of Thr378 is 4.3 Å. A shift in the 380s loop was observed on the T to R transition (Barford et al., 1992) which was correlated with a change of subdomain orientation at the entrance to the catalytic site and a break in an important interdomain ionic contact between Glu382 and Arg770. The further shift in this region observed in the R state complexed structure provides an extra contribution to the glucosyl recognition site. The 380s loop provides a link between the catalytic site and the glycogen storage site (Barford et al., 1992).

Comparison of the R State and T State GPb−NJT−Phosphate Complexes. Comparison of the positions of the catalytic site residues that form the glucosyl and phosphate recognition sites and the positions of the NJT and phosphate molecules in the T and R state complexes shows there is very little difference between them (Figure 6). The positions

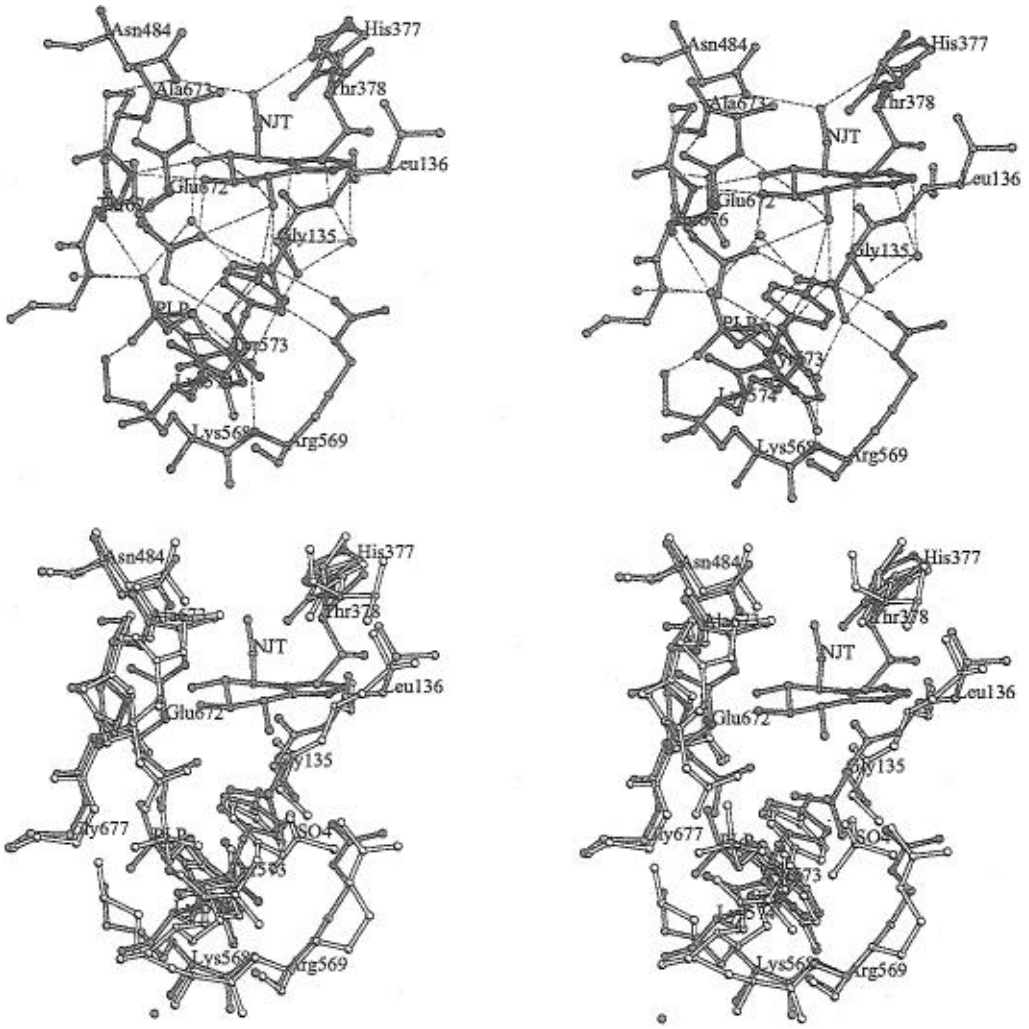

FIGURE 5: Contacts between NJT and phosphate and protein groups at the catalytic site for the R state GPb−NJT−phosphate complex. (a, top) Subunit 1 of the GPb−NJT−phosphate complex. The color scheme is the same as in Figure 3. (b, bottom) Comparison with the native R state structure (white bonds) in which a sulfate ion (SO_4) is bound at the catalytic site and the complexed structure in which Arg569 occupies the position of the sulfate and makes close contacts with the phosphate ion. The shift in Thr378 is apparent.

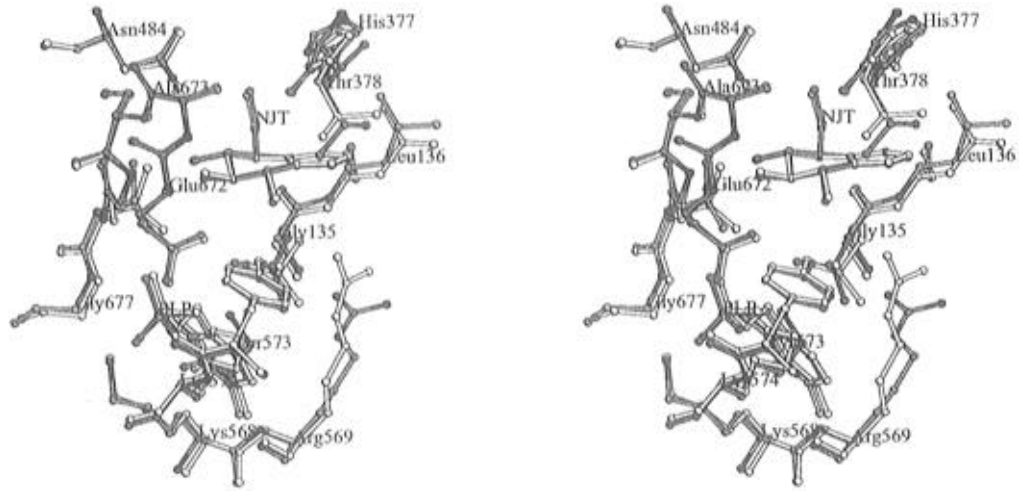

FIGURE 6: Comparison between the T (white bonds) and R state GPb−NJT−phosphate complexes. The two structures are similar. Contacts between Arg569 and the phosphate are stronger in the R state.

of substrate phosphate oxygens determined from the lower resolution room temperature T state (2.4 Å resolution) and R state (2.5 Å resolution) structures are consistent with those established from the 100 K T state ternary complex at 1.7 Å resolution. The ($2F_o - F_c$) map of the refined R state model gave indications of hydrogen bonds between the phosphate and surrounding residues and supports the T state phosphate orientation. After superposition the average difference in the phosphorus atoms of the phosphate ions is 0.26 Å, which is within the experimental error of the model.

Overall, there are substantial differences between the T and R state complexed structures that are typical of the T to R transition. The overall rms difference for 781 atoms is 0.92 Å. These differences affect subunit−subunit contacts

and other regions of the molecule that have already been described (Barford et al., 1992). The major difference between the T and R state complexed structures at the catalytic site occurs in the 280s loop. In the T state ternary complex, this loop is displaced but exhibits some order. In the R state complex, the loop has no apparent order. In both T and R state complex structures, the positive electrostatic pocket formed by Lys568, Arg569, Lys574, and the tetrazole provides the phosphate recognition site and allows proximity of substrate phosphate and PLP 5′-phosphate. The contacts from the side chain of Arg569 are stronger in the R state where the guanidinium group engages the substrate phosphate with two hydrogen bond contacts. In the R state Arg569 is well located, but in the T state the residue is more mobile, perhaps as a result of the conformational change that takes place on formation of the ternary complex and the restriction on the full activation response because of lattice contacts. There is also a small difference in the loop residues 133−136, and this is correlated with the break in hydrogen bonds of Arg569 to Asn133 on activation.

The refined R state GPb−NJT−phosphate complex structure at 2.5 Å resolution has a total of 252 waters per subunit added to the model. The resolution of the original R state GPb structure was insufficient to locate water molecules, and hence this study allows a description of the waters and their role in stabilization of structure and ligand complexes. Out of the total of 252 waters, 130 are open to solvent to some degree and 122 are buried within the protein structure. Some of the highest peaks in the Fourier map used to place these waters corresponded to waters at the catalytic site. The catalytic site waters are well ordered with an average *B* factor of 18 Å^2 compared to the average *B* factor of 14 Å^2 for catalytic site residue Cα atoms. A comparison of the water structure of the T state and R state GPb−NJT−phosphate complexes shows 86 (34%) structurally equivalent water molecules whose superimposed positions are within 1.0 Å and 46 (18%) waters with positions within 0.5 Å. Of the 86 conserved waters 65 (76%) of them are buried within the protein structure with no solvent access.

The contacts from the enzyme to the phosphate ion, including those from the conserved shell of waters surrounding the 5′-phosphate, are very similar in the T and R state complexes. Two waters are located between the substrate phosphate and PLP 5′-phosphate, making contacts to protein and ligands identical to those of the equivalent waters in the T state (Figure 3c). These waters contribute, together with the surrounding protein, to stabilization of the phosphate−phosphate interaction. Other active site waters mediate contacts between NJT, pyridoxal phosphate, and the protein. The shell of five waters surrounding the 5′-phosphate makes contacts to all the phosphate oxygens and a bridge to the surrounding protein residues Val567, Arg569, Tyr648, Glu665, and Asn678. The conservation of waters at the active site suggests that they play an important role in maintaining the active site structure and in promoting the positioning and orientation of substrates.

Comparison with Glc-1-P, Heptenitol, and Heptulose 2-Phosphate. Many ligand binding studies have been carried out with GP over the years. The most relevant for the present work are those with the binary complexes with the substrate Glc-1-P in both the T and the R states (Martin et al., 1990; Johnson et al., 1992), the time-resolved studies with heptenitol and phosphate (Duke et al., 1992), and detailed studies on the product heptulose 2-phosphate (Johnson et al., 1990).

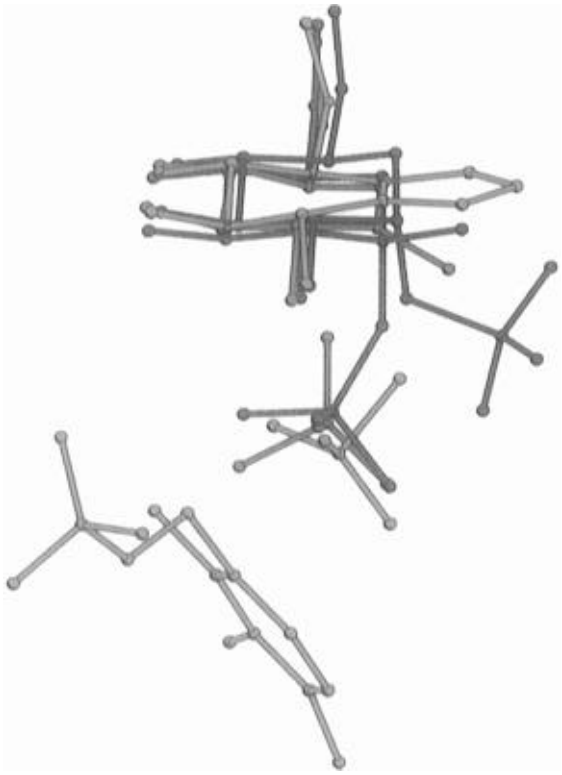

FIGURE 7: Comparison of the T state NJT and phosphate (green) positions with those for heptulose 2-phosphate (magenta), heptenitol and phosphate from the time-resolved studies (red), and Glc-1-P (blue). The PLP position in the GPb−NJT−phosphate complex is shown for reference.

The structures are shown superimposed in Figure 7. The positions of the glucosyl components of each of the structures are similar, indicating that the glucosyl recognition site does not change substantially on activation and nor are there significant differences between the recognition of a glucose-like molecule with an sp^3 hybridized carbon at C1 (Glc-1-P and heptulose 2-phosphate) or an sp^2 hybridized carbon (heptenitol and NJT). The largest difference in positions of glucosyl atoms in Glc-1-P and NJT is in their C1 positions which differ by 0.6 Å, a difference which reflects the chair geometry of Glc-1-P and the half-chair geometry of NJT. Other atoms differ by less than 0.4 Å. With heptulose 2-phosphate the glucosyl ring is 0.5 Å toward the phosphate position compared with NJT. This represents an apparent compromise on the part of heptulose 2-phosphate to accommodate both the glucosyl ring and the covalently bound phosphate.

The phosphate recognition sites of these liganded complexes show variation. In the Glc-1-P complexes in both T and R states the conformation about the C1−O glycosidic linkage (torsion angle O5−C1−O1−P) is 152°, which is similar to the preferred conformation found in the single crystal structure of Glc-1-P and also similar to that observed for α-1,4-linked oligosaccharides (Martin et al., 1990). In this conformation, the phosphate group is not in contact with the cofactor 5′-phosphate and is not in a correct position to promote catalysis. In contrast, in heptulose 2-phosphate the additional methyl group linked in the β configuration at C1 promotes a change in the glycosidic torsion angle to 224°. The product phosphate is within hydrogen-bonding distance of the cofactor 5′-phosphate in what is likely to be a location close to that adopted by the phosphate during reaction (Johnson et al., 1990). The time-resolved Laue experiments and experiments with low phosphate concentrations with

heptenitol had succeeded in identifying a putative phosphate group bound close to this position (Duke et al., 1994). The position was consistent with the position of a phosphate group about to attack the heptenitol. This conclusion is substantiated by the present results with NJT and phosphate. In the present work, the position of the phosphate group is unambiguous. It is firmly bound and makes a substantial number of contacts with groups on the enzyme, through water molecules and direct contacts to both NJT and to the cofactor 5′-phosphate. The position of the phosphates in the T and R state NJT complexes are 0.55 and 0.39 Å, respectively, from the phosphate position observed in the time-resolved experiments on the conversion of heptenitol to heptulose 2-phosphate. The phosphate position in the T state NJT complex is 0.79 Å from its position in the heptulose 2-phosphate complex and 3.2 Å from the phosphate of Glc-1-P. In both the T state NJT−phosphate complex and the T state heptulose 2-phosphate complex there is a mutual interchange of Asp283 and Arg569 and a shift of the 280s loop.

DISCUSSION

Kinetic Studies and Implications for the Transition State. NJT functions as a competitive inhibitor with respect to Glc-1-P with a K_i value of 700 μM when binding to the phosphorylase−glycogen−AMP complex. However, in the presence of phosphate, the binding improves by over an order of magnitude (13-fold). Uncompetitive inhibition is observed with respect to phosphate, and a K_i value of 53 μM for the phosphorylase−glycogen−AMP−phosphate complex is found. The competitive inhibition with respect to Glc-1-P is consistent with the two sugar analogues competing for the catalytic site, while the observation of uncompetitive inhibition when phosphate is the variable substrate implies that the NJT binding site does not overlap significantly with the phosphate site since the two can bind at the same time. The interpretation of the kinetic data as indicating uncompetitive inhibition implies that there should be no binding of NJT to the free enzyme, only to the enzyme−phosphate complex. This would appear to be inconsistent with the crystallographic observation of NJT bound to the catalytic site in the absence of phosphate. However, the crystallographic experiments in the absence of phosphate were carried out at a concentration of NJT at 100 mM, which is much higher than that used in the kinetic experiments. Under these conditions it is probable that NJT binding to the free enzyme is observed. Alternatively, the results could be interpreted in terms of mixed inhibition, which would allow for this possibility. This does not in any way alter the main conclusion of the kinetic studies that phosphate dramatically improves the affinity for NJT.

These results are similar to those of Gold et al. (1971) on the binding of D-gluconolactone to GPa. In their work it was found that binding of either glycogen or phosphate enhanced the affinity of the free enzyme for 5-gluconolactone by a factor of more than 10, and binding of phosphate enhanced the affinity of the GPa−glycogen complex a further 28-fold to give a $K_i = 25$ μM for the enzyme−glycogen−phosphate complex. Both D-gluconolactone and NJT exhibit weak binding by themselves, which indicates that the structural and electrostatic consequences of an sp^2 hybridized carbon at C1 and the resulting half-chair geometry of the glucopyranose ring do not by themselves confer transition state-like properties that lead to tight binding. However, the increase in affinity observed in the presence of phosphate indicates that it is the combination of sp^2 hybridization and the phosphate that has the elements of a transition state analogue. Such an increase in affinity is not observed for inhibitors with sp^3 hybridized C1 atoms, such as glucose, in the presence of phosphate. Indeed, such binding is mutually exclusive. It must however be present at the transition state for oligosaccharide or glycogen substrates since efficient turnover occurs. Similar synergistic binding of two components to give a transition state analogue inhibitor was observed in squalene synthetase (Sandifer et al., 1982).

Creation of the Phosphate Recognition Site. What are the molecular contacts that lead to synergistic binding? In native T state crystals the phosphate recognition site is not fully developed. Phosphate does not bind at the catalytic site even at high (0.5 M) concentrations. The kinetic studies have shown that phosphate tightens the binding of NJT, and the X-ray experiments show that NJT tightens the phosphate recognition site; thus there is synergy between the two ligands. Other crystallographic studies show that there is no such synergy and no appreciable phosphate binding in the presence of a glucosyl compound in the chair conformation (Mitchell, 1995).

The two contacts between NJT and phosphate, the O-2 to OP-1 hydrogen bond and N-1 to OP-1 contact, appear important in establishing the synergy between ligand and phosphate. The contact from the N-1 of NJT to the OP-1 of the phosphate could represent either a hydrogen bond interaction if the phosphate oxygen was protonated, as modeled in the X-ray studies, or a charge−charge interaction if the OP-1 oxygen was negatively charged and considering the polar nature of the tetrazole ring, as expressed by one of the canonical forms shown in Figure 1. The O-2 hydroxyl group of glucosyl substrates is important for catalysis as demonstrated by Street et al. (1989) in kinetic analysis with deoxyfluoroglucose-1-P analogues and by Becker et al. (1994) in mutational studies with *Escherichia coli* maltodextrin phosphorylase and also as discussed by Duke et al. (1994). The contact of O-2 to the active site residues Tyr573 and Glu672 is important in locating the glucosyl ligand and the contact from O-2 to phosphate in locating the phosphate in the correct orientation for catalysis. However, since the O-2 contact is available to glucose and other glucopyranosyl compounds that do not stabilize the phosphate binding in the T state, we conclude that it is the contact between the tetrazole ring and phosphate that is the more important determinant for synergistic binding.

In the R state the phosphate recognition site is already available, and the side chain of Arg569 makes important contributions. In the T state the binding of phosphate in the presence of NJT at the catalytic site can favor movement of Arg569 into the catalytic site, as was observed previously in the study of heptulose 2-phosphate. However, it appears that movement of Arg569 is not obligatory for binding of phosphate provided that NJT is present because, in the experiments at 100 K, phosphate bound without movement of the arginine. The contributions of the other basic groups in the vicinity, Lys568 for the stabilization of the cofactor phosphate and Lys574 for the inorganic phosphate, together with the main chain NH contributions from Thr676 and Gly677 for the cofactor phosphate and Gly135 for inorganic phosphate, are important but insufficient by themselves to promote the binding of inorganic phosphate. Either NJT or Arg569 is needed to create the phosphate recognition site,

and presumably when both are present, as in the R state GPb−NJT−phosphate complex, the binding site is optimal.

The importance of creating the correct phosphate recognition site arises from the fact that this site is close to the cofactor 5′-phosphate and special interactions are required to bring the two phosphate groups together. In both the T and R state GPb−NJT−phosphate complexes there is a hydrogen bond between the 5′-phosphate of the PLP and the inorganic phosphate. This interaction is consistent with proposals for an essential role of the cofactor phosphate in the promotion of catalysis. The negative charge density of the two interacting phosphate ions is compensated by the surrounding basic residues Lys568, Lys574, and Arg569 and contributions from main chain NH groups.

It is interesting that the sulfate position occupied at the catalytic site of R state GPb and GPa (where the crystals were grown in the presence of ammonium sulfate) and the phosphate position occupied in the R state NJT−phosphate complex differ by 2.5 Å. Work with triosephosphate isomerase has shown that sulfate and phosphate binding sites may not be identical (Verlinde et al., 1991). On the basis of their studies with sulfate and phosphate binding proteins, Quiocho and colleagues have concluded that while both dianions require hydrogen bonding (but not necessarily basic groups) to stabilize their binding, sulfate oxygen atoms can only participate as acceptors in such interactions whereas one phosphate oxygen atom can participate as a donor if required (Quiocho et al., 1987; Luecke & Quiocho, 1990). In GP the reason for the differences in positions of the sulfate and phosphate ions is not obvious since both participate in interactions with the 5′-phosphate of the cofactor and the basic groups Arg569 and Lys574. A possible explanation is that the phosphate is drawn into its position by the additional interactions with NJT, although this has not been tested.

Catalytic Mechanism. Transition from the T to R state in GP results in both an increase in affinity for the substrate phosphate and an increase in activity. The structural studies on the T and R state GPb−NJT−phosphate complexes have provided evidence for the location of the substrate phosphate binding site. They also confirm that there is direct interaction between the PLP 5′-phosphate and the substrate phosphate. The high-resolution 1.7 Å studies have allowed a definitive description of the orientation of the two phosphate groups. They show that the phosphates are in optimal orientation for a direct hydrogen-bonding arrangement. This disposition is consistent with the proposed role for the cofactor phosphate as a general acid in the catalytic mechanism. Modeling of the catalytic site, with the terminal glucose of an oligosaccharide placed over the NJT sugar position, shows OP-1 of the phosphate to be in a position to donate a proton to the glycosidic bond (Figure 8). We note however that the static picture obtained from X-ray observations does not rule out other possible mechanisms involving interaction between the two phosphates.

An important mechanistic question is the means by which the developing oxocarbonium ion is stabilized. In the "retaining" glycosidases a suitably disposed carboxylate group from a glutamic or aspartic acid usually fulfils this role. No such side chain is apparent in the correct position in glycogen phosphorylase. The structural results have indicated that the phosphate ion itself is likely to contribute significantly to the stabilization. However, it is interesting that the main chain carbonyl oxygen of His377 is appropriately located adjacent to the "anomeric" carbon (C-1) of NJT (Figure 8). This could also contribute to stabilization of the intermediate. Participation by an uncharged group may well be required for an enzyme using a charged substrate, in much the same way that the charged acid catalyst in a β-glucosidase is replaced by a neutral residue in the analogous myrosinase, an enzyme that hydrolyzes a charged substrate (Wang & Withers, 1995). Substrate-assisted catalysis has been proposed for the plant chitinase hevamine for the hydrolysis of chitin based on the crystal structure of the chitinase with allosamidin (Terwisscha van Scheltinga et al., 1995). In hevamine the catalytic site contains no suitably disposed carboxylate group to function as a nucleophile, and it is proposed that the positive charge at C-1 is stabilized intramolecularly by the carbonyl oxygen of the *N*-acetyl group at C-2.

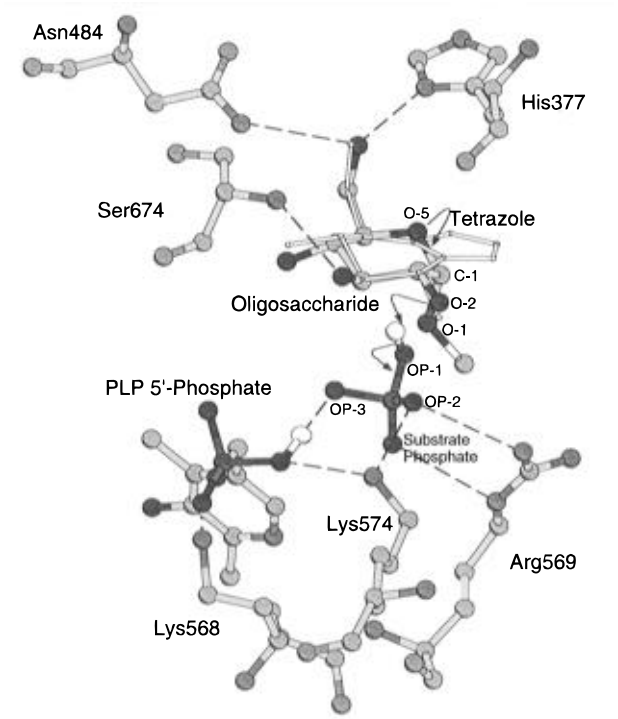

FIGURE 8: Schematic diagram of the catalytic site of GPb illustrating the relative orientations of selected residues and the PLP 5′-phosphate group to the substrate (modeled as a glycoside) and phosphate (as observed in the present work). NJT is shown with thin lines for reference. The position of the carbonyl oxygen of His377, which may play a role in the stabilization of the oxocarbonium ion transition state, is shown. For clarity, side chains in contact with the O-2 hydroxyl, which are important for specificity and catalysis and are shown in Figure 5, are omitted here, and hydrogen atoms are only indicated for the active phosphate oxygen groups.

Summary. The work has shown that NJT can contribute to the creation of the substrate phosphate recognition site and that there are mutual interactions in which NJT stabilizes the phosphate binding and phosphate promotes NJT binding. The phosphate ion bound in this position is correctly disposed to attack the substrate in a reaction that is promoted by the 5′-phosphate group of the cofactor PLP. The results confirm the phosphate position identified previously in time-resolved studies and suggest a possible mechanism for stabilization of the glycosyl−enzyme intermediate.

ACKNOWLEDGMENT

We wish to acknowledge the contributions of the staff at SRS, Daresbury, for their help in data collection and the

assistance with computing in the Laboratory of Molecular Biophysics from Dr. R. Bryan and Dr. R. Esnouf. We are grateful to Dr. M. E. M. Noble for production of Figures 3, 5, 6, and 7 with the program XOBJECTS.

REFERENCES

Acharya, K. R., Stuart, D. I., Varvill, K. M., & Johnson, L. N. (1991) *Glycogen phosphorylase: Description of the protein structure*, World Scientific, London and Singapore.

Ariki, M., & Fukui, T. (1977) *J. Biochem. 81*, 1017−1024.

Ashwell, G. (1957) *Methods Enzymol. 3*, 73−105.

Barford, D., & Johnson, L. N. (1989) *Nature 340*, 609−614.

Barford, D., & Johnson, L. N. (1992) *Protein Sci. 1*, 472−493.

Barford, D., Schwabe, J. W. R., Oikonomakos, N. G., Acharya, K. R., Hajdu, J., Papageorgiou, A. C., Martin, J. L., Knott, J. C. A., Vasella, A., & Johnson, L. N. (1988) *Biochemistry 27*, 6733−6741.

Barford, D., Hu, S.-H., & Johnson, L. N. (1991) *J. Mol. Biol. 218*, 233−260.

Becker, S., Palm, D., & Schinzel, R. (1994) *J. Biol. Chem. 269*, 2485−2490.

Bichard, C. J., Mitchell, E. P., Wormald, M. R., Watson, K. A., Johnson, L. N., zographos, S. E., Koutra, D. D., Oikonomakos, N. G., & Fleet, G. W. J. (1995) *Tetrahedron Lett. 36*, 2145−2148.

Brunger, A. T. (1992) *X-PLOR: Version 3.1; a system for protein crystallography and NMR*, Yale University Press, New Haven, CT.

Conchie, J., & Levvy, G. A. (1957) *Biochem J. 65*, 389−392.

Copley, R., & Barton, G. J. (1994) *J. Mol. Biol. 242*, 321−329.

Cosier, J., & Glazer, A. M. (1986) *J. Appl. Crystallogr. 19*, 105−107.

Duke, E. M. H., Hadfield, A., Wakatsuki, S., Bryan, R. K., & Johnson, L. N. (1992) *Philos. Trans. R. Soc. London A 340*, 245−261.

Duke, E. M. H., Wakatsuki, S., Hadfield, A., & Johnson, L. N. (1994) *Protein Sci. 3*, 1178−1196.

Engers, H. D., Shechosky, S., & Madsen, N. B. (1970) *Can. J. Biochem. 48*, 746−754.

Engh, R. A., & Huber, R. (1991) *Acta Crystallogr. A47*, 392−400.

Ermert, P., & Vasella, A. (1991) *Helv. Chim. Acta 74*, 2043−2053.

Ermert, P., Vasella, A., Weber, M., Rupitz, K., & Withers, S. G. (1993) *Carbohydr. Res. 250*, 113−128.

Fischer, E. H., & Krebs, E. G. (1962) *Methods Enzymol. 5*, 369−372.

Gold, A. M., Legrand, E., & Sanchez, G. R. (1971) *J. Biol. Chem. 246*, 5700−5706.

Goldsmith, E. J., Sprang, S. R., Hamlin, R., Xuong, N.-H., & Fletterick, R. F. (1989) *Science 245*, 528−532.

Graves, D. J., & Wang, J. H. (1972) α-Glucan phosphorylases−chemical and physical basis of catalysis and regulation, *The Enzymes* (Boyer, P. D., Ed.) 3rd ed.; pp 435−482, Academic Press, New York.

Hadju, J., Acharya, K. R., Stuart, D. I., McLaughlin, P. J., Barford, D., Oikonomakos, N. G., Klein, H., & Johnson, L. N. (1987) *EMBO J. 6*, 539−546.

Hanozet, G., Pircher, H.-P., Vanni, P., Oesch, B., & Semenza, G. (1981) *J. Biol. Chem. 256*, 3703−3711.

Howard, A. J., Gilliland, G. L., Finzel, B. C., Poulos, T. L., Ohlendorf, D. H., & Salemme, F. R. (1987) *J. Appl. Crystallogr. 20*, 383−387.

Hu, S.-H. (1992) *Crystallographic studies on activated glycogen phosphorylase*, University of Oxford, Oxford.

Johnson, L. N. (1992) *FASEB J. 6*, 2274−2282.

Johnson, L. N., Hajdu, J., Acharya, K. R., Stuart, D. I., McLaughlin, P. J., Oikonomakos, N. G., & Barford, D. (1989) Glycogen phosphorylase b, *Allosteric Enzymes* (Herve, G., Ed.) pp 81−127, CRC Press, Boca Raton, FL.

Johnson, L. N., Acharya, K. R., Jordan, M. D., & McLaughlin, P. J. (1990) *J. Mol. Biol. 211*, 645−661.

Johnson, L. N., Hu, S.-H., & Barford, D. (1992) *Faraday Discuss. 93*, 131−142.

Jones, T. A. (1985) *Methods Enzymol. 115*, 157−171.

Jones, T. A., Zou, J. Y., Cowan, S. W., & Kjeldgaard, M. (1991) *Acta Crystallogr. A47*, 110−119.

Kabsch, W. (1993) *J. Appl. Crystallogr. 26*, 795−800.

Leatherbarrow, R. J. (1992) *Enzfitter: A Non-linear Regression Data Analysis Program*. Grafit Version 3.0, Erithakus Software, Staines, U.K.

Leonidas, D. D., Oikonomakos, N. G., Papageorgiou, A. C., & Sotiroudis, T. G. (1992) *Protein Sci. 1*, 1123−1132.

Luecke, H., & Quiocho, F. A. (1990) *Nature 347*, 402−406.

Martin, J. L., Withers, S. G., & Johnson, L. N. (1990) *Biochemistry 29*, 10745−10757.

Martin, J. L., Veluraja, K., Ross, K., Johnson, L. N., Fleet, G. W. J., Ramsden, N. G., Bruce, I., Orchard, M. G., Oikonomakos, N. G., Papageorgiou, A. C., Leonidas, D. D., & Tsitoura, H. S. (1991) *Biochemistry 30*, 10101−10116.

McLaughlin, P. J., Stuart, D. I., Klein, H. W., Oikonomakos, N. G., & Johnson, L. N. (1984) *Biochemistry 23*, 5862−5873.

Mitchell, E. P. (1995) *Cryocrystallographic and mechanistic studies on glycogen phosphorylase*, University of Oxford, Oxford.

Mitchell, E. P., & Garman, E. F. (1994) *J. Appl. Crystallogr. 27*, 1070−1074.

Otwinowski, Z. (1993) *DENZO. Data Collection and Processing*, DL/SC1/R34, SERC Laboratory, Daresbury, Warrington, U.K.

Papageorgiou, A. C., Oikonomakos, N. G., Leonidas, D. D., Bernet, B., Beer, D., & Vasella, A. (1991) *Biochem. J. 274*, 329−338.

Parrish, R. J., Uhing, R. J., & Graves, D. J. (1977) *Biochemistry 16*, 4824−4831.

Quiocho, F. A., Sack, J. S., & Vyas, N. K. (1987) *Nature 329*, 561−564.

Read, R. J. (1986) *Acta Crystallogr. A42*, 140−149.

Sandifer, R. M., Thompson, M. D., Gaughan, R. G., & Poulter, C. D. (1982) *J. Am. Chem. Soc. 104*, 7376−7378.

Sinnott, M. L. (1990) *Chem. Rev. 90*, 1171−1202.

Sprang, S. R., Goldsmith, E. J., Fletterick, R. J., Withers, S. G., & Madsen, N. B. (1982) *Biochemistry 21*, 5364−5371.

Sprang, S. R., Withers, S. G., Goldsmith, E. J., Fletterick, R. J., & Madsen, N. B. (1991) *Science 254*, 1367−1371.

Street, I. P., Rupitz, K., & Withers, S. G. (1989) *Biochemistry 28*, 1581−1587.

Teng, T.-Y. (1990) *J. Appl. Crystallogr. 23*, 387−391.

Terwisscha van Scheltinga, A. C., Armand, S., Kalk, K. H., Isogai, A., Henrissat, B., & Dijstra, B. W. (1995) *Biochemistry 34*, 15619−15623.

Uhing, R. J., Janski, A. M., & Graves, D. J. (1979) *J. Biol. Chem. 254*, 3166−3169.

Verlinde, C. L. M. J., Noble, M. E. M., Kalk, K. H., Groendijk, H., Wierenga, R. K., & Hol, W. G. J. (1991) *Eur. J. Biochem. 198*, 53−57.

Wang, Q., & Withers, S. G. (1995) *J. Am. Chem. Soc. 117*, 10137−10138.

Watson, K. A., Mitchell, E. P., Johnson, L. N., Son, J. C., Bichard, C. J. F., Orchard, M. G., Fleet, G. W. J., Oikonomakos, N. G., Leonidas, D. D., Kontou, M., & Papageorgiou, A. C. (1994) *Biochemistry 33*, 5745−5758.

Watson, K. A., Mitchell, E. P., Johnson, L. N., Crucianni, G., Son, J. C., Bichard, C. J. F., Fleet, G. W. J., Oikonomakos, N. G., Leonidas, D. D., & Kontou, M. (1995) *Acta Crystallogr. D51*, 458−472.

Withers, S. G., Madsen, N. B., Sprang, S. R., & Fletterick, R. F. (1982) *Biochemistry 21*, 5372−5382.

Withers, S. G., Madsen, N. B., Sykes, B. D., Takagi, M., Shimomura, S., & Fukui, T. (1981) *J. Biol. Chem. 256*, 10759−10762.

BI960072W